

# Processing and magneto-electric properties of sol-gel-derived $\text{Pb}(\text{Zr}_{0.52}\text{Ti}_{0.48})\text{O}_3\text{-Ni}_{0.8}\text{Zn}_{0.2}\text{Fe}_2\text{O}_4$ 2-2 type multilayered films

Li Wang · Ruzhong Zuo · Hailin Su ·

Min Shi · Yudong Xu · Guang Wu ·

Guizhang Yu

Received: 31 December 2010 / Accepted: 15 March 2011 / Published online: 29 March 2011  
© Springer Science+Business Media, LLC 2011

**Abstract**  $\text{Pb}(\text{Zr}_{0.52}\text{Ti}_{0.48})\text{O}_3\text{-Ni}_{0.8}\text{Zn}_{0.2}\text{Fe}_2\text{O}_4$  (PZT–NZFO) multilayered thin films with various volume fractions of the PZT phase (100, 74, 58, 48, 33, and 0%) were prepared on Pt/Ti/SiO<sub>2</sub>/Si substrates using sol–gel spin-coating method. X-ray diffraction shows polycrystalline structure and scanning electron microscopy reveals good multilayer morphology of the composite thin film as annealed at 700 °C in air. The thickness of the composite films was estimated in the range of ~400 to ~600 nm. The ferroelectric and magnetic properties were measured as function of the volume fractions of the PZT phase. The magnetoelectric (ME) effect was investigated under various bias magnetic fields. The maximum ME voltage coefficient ( $\alpha_E = dE/dH$ ) is 278 mV/cmOe for the composite film with the volume fractions of the PZT phase of ~48%.

## Introduction

A great deal of attention has been paid to multiferroic materials because of their significant potential applications in the novel multifunctional devices such as transducers, sensors, and so on. These materials can not only display ferroelectric and magnetic properties simultaneously, but also have a magnetoelectric (ME) effect that is a

spontaneous dielectric polarization of a material in an applied magnetic field and/or an induced magnetization in an external electric field [1–4]. In recent years, much attention has been paid to magnetoelectric nanocomposite films [5–7]. Compared to bulk composites, ME nanocomposite thin films exhibit some unique advantages. Their phase composition and connectivity could be controlled at nanometer scale, which have potential applications in micro/nano devices [8]. For composite ME materials preparation, individual components should have high ferroelectric and magnetic properties. In this view, one of the most preferred choices should be PZT as ferroelectric phase and Ni–Zn ferrite as ferromagnetic phase. Srinivasan et al. [9] reported that low anisotropy and high permeability caused by doping Zn is favorable to the magnetomechanical coupling and thus result in a giant ME effect in the  $\text{Pb}(\text{Zr}_{0.52}\text{Ti}_{0.48})\text{O}_3\text{-Ni}_{0.8}\text{Zn}_{0.2}\text{Fe}_2\text{O}_4$  thick films. Up to now, several reports about magnetoelectric composites thin film with different materials, including magnetostrictive ones of  $\text{MnFe}_2\text{O}_4$ ,  $(\text{Co}, \text{Ni})\text{Fe}_2\text{O}_4$ ,  $(\text{La}, \text{Sr})\text{MnO}_3$ , Terfenol-d, etc., and piezoelectric ones of PZT,  $\text{BaTiO}_3$ ,  $\text{SrBi}_4\text{Ti}_4\text{O}_{15}$ ,  $(\text{Sr}, \text{Ba})\text{Nb}_2\text{O}_6$ , etc., have been published [10–15]. Usually, particle composite thin films were prepared by sol–gel spin-coating method [16] or chemical solution deposition [17] and multilayered thin films composed of ferromagnetic and ferroelectric phases were obtained by pulsed laser deposition [18] and rf-magnetron sputtering [19]. However, there were few investigations on sol–gel-derived multilayered thin films of  $\text{Pb}(\text{Zr}_{0.52}\text{Ti}_{0.48})\text{O}_3\text{-Ni}_{0.8}\text{Zn}_{0.2}\text{Fe}_2\text{O}_4$  whose thickness are at nanometer scale.

In our study,  $\text{Pb}(\text{Zr}_{0.52}\text{Ti}_{0.48})\text{O}_3\text{-Ni}_{0.8}\text{Zn}_{0.2}\text{Fe}_2\text{O}_4$  (PZT–NZFO) magnetoelectric multilayered thin films of 2-2 type heterostructure were prepared onto Pt(111)/Ti/SiO<sub>2</sub>/Si substrate by a sol–gel spin-coating technique. The films' ferroelectric, magnetic, and ME properties were investigated.

L. Wang · R. Zuo (✉) · H. Su (✉) · M. Shi · Y. Xu · G. Wu ·  
G. Yu

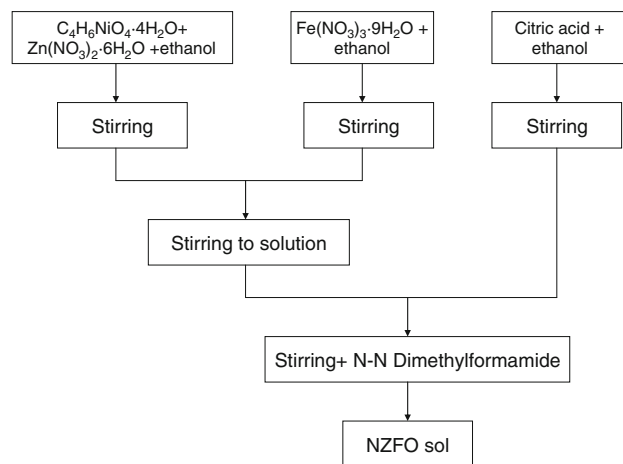
Institute of Electro Ceramics & Devices, School of Materials Science and Engineering, Hefei University of Technology, Hefei 230009, People's Republic of China  
e-mail: piezolab@hfut.edu.cn

H. Su  
e-mail: suhlnju@yahoo.com.cn

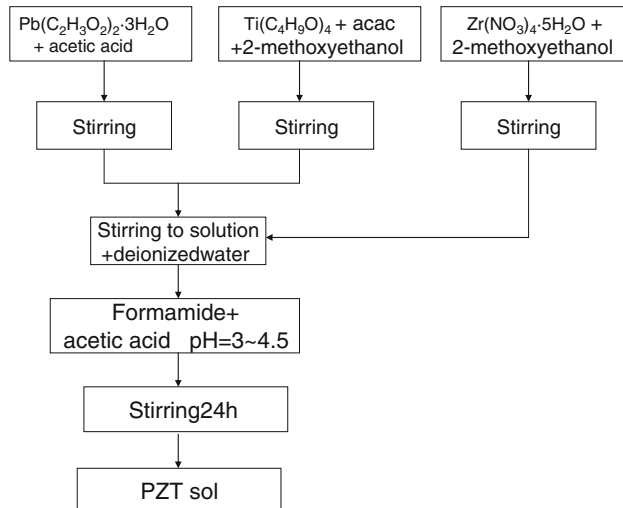
## Experimental

Figure 1 shows the flow charts for preparing the NZFO and PZT sol by the sol–gel process. For the preparation of the NZFO precursor solution, nickel acetate tetrahydrate  $\text{Ni}(\text{CH}_3\text{COO})_2 \cdot 4\text{H}_2\text{O}$ , zinc nitrate hexahydrate  $\text{Zn}(\text{NO}_3)_2 \cdot 6\text{H}_2\text{O}$ , iron nitrate nonahydrate  $\text{Fe}(\text{NO}_3)_3 \cdot 9\text{H}_2\text{O}$ , and citric acid  $\text{C}_6\text{H}_8\text{O}_7 \cdot \text{H}_2\text{O}$  were dissolved in ethanol, respectively. Solution of iron nitrate and Ni–Zn were first mixed together and stirred at room temperature for half an hour. Then citric acid solution was added into above solution and stirred continuously to get a sol precursor solution (0.2 M) of Zn-doped nickel ferrite  $\text{Ni}_{0.8}\text{Zn}_{0.2}\text{Fe}_2\text{O}_4$ . The molecule ratio of Ni:Zn:Fe was 0.8:0.2:2. *N*–*N* dimethylformamide as fraction-control agent was added into the sol precursor solution. The appropriate portions of zirconium nitrate

(a)



(b)



**Fig. 1** Flow charts of preparing NZFO and PZT sol via sol–gel method

pentahydrate  $\text{Zr}(\text{NO}_3)_4 \cdot 5\text{H}_2\text{O}$  and tetrabutyl titanate  $\text{Ti}(\text{C}_4\text{H}_9\text{O})_4$  were dissolved in 2-methoxyethanol, respectively. Lead acetate trihydrate  $\text{Pb}(\text{CH}_3\text{COO})_2 \cdot 3\text{H}_2\text{O}$  was dissolved in acetic acid.  $\text{Ti}(\text{C}_4\text{H}_9\text{O})_4$  solution was added to the  $\text{Pb}(\text{CH}_3\text{COO})_2$  solution with acetylacetone (acac) as chelating agents. Then  $\text{Zr}(\text{NO}_3)_4$  solution was added into above solution and stirred at 80 °C to form precursor solution (0.3 M) of  $\text{Pb}(\text{Zr}_{0.52}\text{Ti}_{0.48})\text{O}_3$ , and 10 mol% excess Pb was used to compensate for the volatile Pb. After aging for 3 days in air, the PZT and NZFO precursor solutions were alternately spin coated onto the substrate to form 2–2 type four-layered nanocomposite precursor films. And the volume fractions of the PZT and NZFO phases within the films were adjusted by changing the spin-coating repeating times of each phase. In this experiment, four multilayered films named  $\text{A}_4\text{B}_1\text{A}_4\text{B}_1\text{A}_1$ ,  $\text{A}_4\text{B}_2\text{A}_4\text{B}_2\text{A}_1$ ,  $\text{A}_4\text{B}_3\text{A}_4\text{B}_3\text{A}_1$ , and  $\text{A}_2\text{B}_3\text{A}_2\text{B}_3\text{A}_1$  were prepared. Here, A stands for PZT, B stands for NZFO, and the number in the subscript stands for the spin-coating repeating times. For these four films, their PZT volume fractions are ~74, 58, 48, and 33%, respectively, and the corresponding total thickness are ~400, ~500, ~600, and ~550 nm, respectively. After each spin-coating step, the films were dried at 200 °C for 3 min and pre-annealed at 400 °C for 5 min to remove organic components. Finally, the precursor films obtained by repeating the spin-coating-drying-preannealing process were annealed in air at 700 °C for 15 min in the tube furnace.

The films were characterized using X-ray diffraction (XRD, D/Mzx-rB, Rigaku) using  $\text{Cu K}_\alpha$  radiation. The surface and cross-section morphologies of the thin films were assessed by field emission scanning electron microscopy (FE-SEM, Sirion200). Electric characterization was carried out on a ferroelectric measuring system (Precision LC) at the frequency of 1 kHz. Punctate Au electrodes with a diameter of 500  $\mu\text{m}$  were deposited through a shadow mask on the composite thin films for electric measurement. Superconducting quantum interference device (SQUID, MPMSXL-7) magnetometer was used to characterize the magnetic properties of the films in the field applied parallel to the film's surface. As for the ME measurement, the ac magnetic field  $H_{\text{ac}}$  (11 Oe) with the frequency of 50 kHz was produced from a sync signal using a solenoid. The ac magnetic field was superimposed onto a dc magnetic field  $H_{\text{dc}}$  up to 5 kOe. The induced voltage in magnetic field was measured using a lock-in amplifier (SRS Inc., SR830).

## Results and discussion

Figure 2 depicts the typical XRD pattern of the multilayered composite PZT–NZFO film with ~33% PZT as well as the patterns of single-phase PZT and NZFO films. The

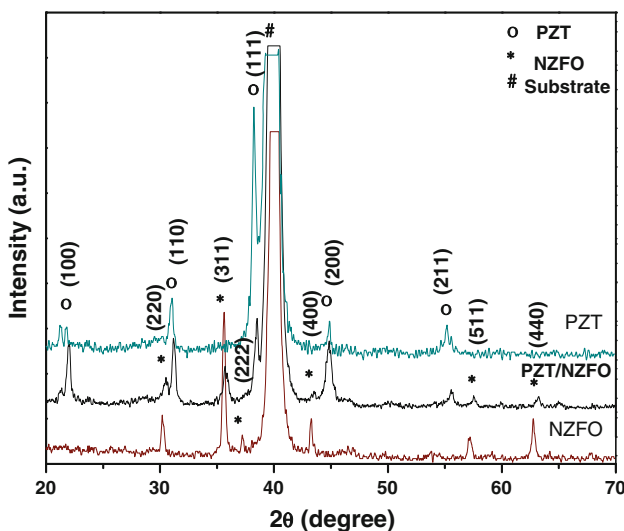
XRD patterns indicate that the composite film consists of PZT and NZFO phases without any additional or intermediate phase. Both the NZFO and PZT phases are polycrystalline structures and do not exhibit preferentially crystallographic orientation. According to single-phase PZT film diffraction peaks, the structural parameters were refined by the Rietveld method using a Maud software. The reliability factor  $R_{wp}$  and the goodness-of-fit indicator  $S$  are 10.62 and 1.48, respectively. The calculated lattice parameters are  $4.034 \pm 0.003 \text{ \AA}$  ( $a = b$ ) and  $4.142 \pm 0.004 \text{ \AA}$  ( $c$ ) which are similar to those of the unstrained  $\text{Pb}(\text{Zr}_{0.52}\text{Ti}_{0.48})\text{O}_3$  ( $a = b = 4.036 \text{ \AA}$  and  $c = 4.146 \text{ \AA}$ ) bulk. This implies that the PZT layer on the Pt/Ti/SiO<sub>2</sub>/Si substrate could help to relieve the stress effect of the substrate due to the small lattice mismatch between Pt ( $a = 3.924 \text{ \AA}$ ) and PZT [11, 12]. Therefore, PZT, not NZFO ( $a = 8.365 \text{ \AA}$ ), was selected as the underlayer for PZT–NZFO multilayered film. By comparing the XRD patterns of composite thin films with those of the two single-phase films, the diffraction peaks of the composite films seems to shift to higher angles, which mainly comes from the NZFO phase. The peak shift of the NZFO phase may be attributed to its lattice contraction caused by the compressive stress state of the NZFO phase with a relatively large lattice constant. It is not clear why the diffraction peak of PZT phase is less sensitive.

Figure 3a and c show the SEM images of the surface and the cross-section for the single-layered NZFO thin film. It can be seen that the film has an uniform and crack-free nano-grain microstructure, whose average grain diameter and thickness are estimated to be  $\sim 40$  and  $\sim 50 \text{ nm}$ , respectively. Figure 3b and d display the SEM

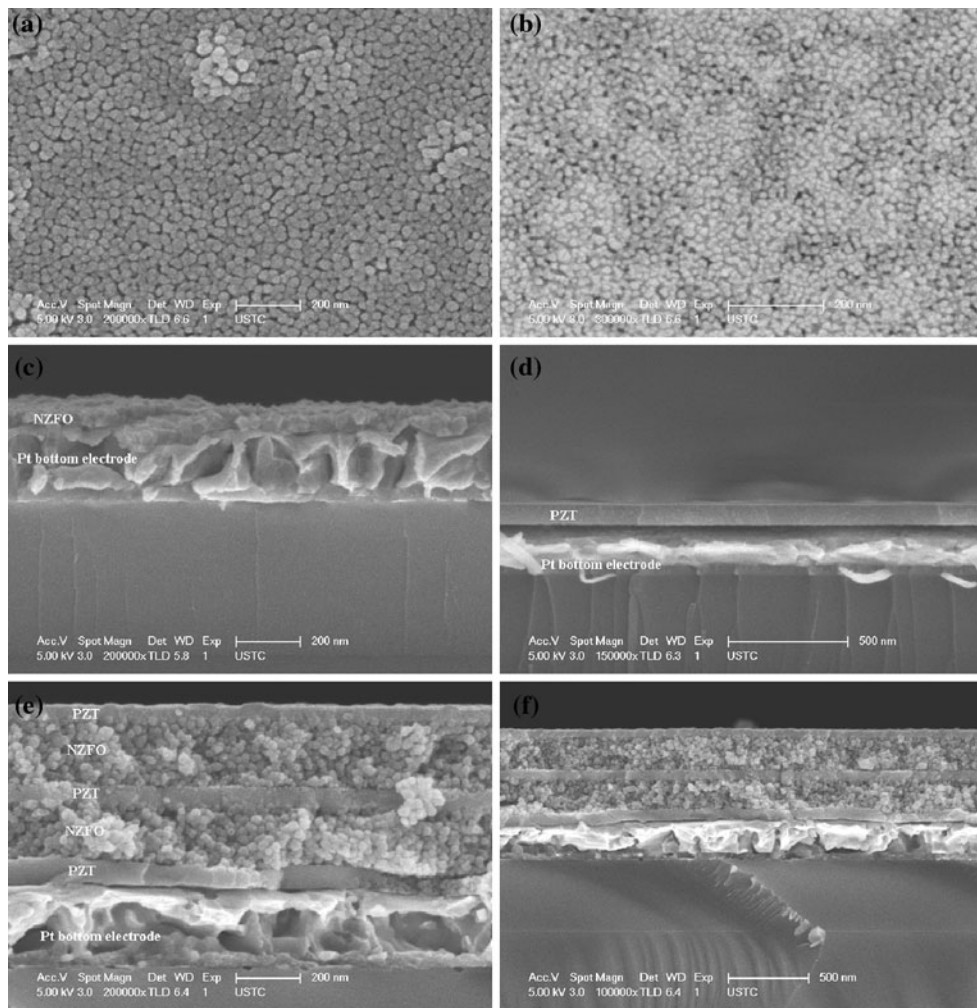
images of the surface and cross-section of the single-layered PZT thin film. The PZT thin film exhibits a high density and uniform microstructure. Its grain size and thickness are  $\sim 20$  and  $\sim 85 \text{ nm}$ , respectively. Comparing Fig. 3c and d, we can see that it is difficult to identify the layer boundary between the substrate and the NZFO film, while the boundary between the PZT film and the substrate is clear and flat. This suggests that there is no diffusion at the interface between the PZT film and substrate. Therefore, the PZT phase was deposited on the substrate first for the multilayered PZT–NZFO films to avoid the diffusion and contribute to weakening the clamping effect of the substrate.

Figure 3e and f show cross-section SEM micrographs of the PZT–NZFO composite thin film with  $\sim 33\%$  PZT. It is clear that the film has a multilayered nanostructure and distinct interface between the PZT layer and the NZFO layer. Both PZT and NZFO layers are relatively uniform in the thickness. The total thickness of the film is estimated to be  $\sim 550 \text{ nm}$ , including  $\sim 180 \text{ nm}$  PZT and  $\sim 370 \text{ nm}$  NZFO. According to the relative thickness of the two phases, the volume fractions of the PZT phase in the composite films are estimated to  $\sim 33\%$ .

The  $P$ – $E$  hysteresis loops of the composite thin films with four different volume fractions of PZT phase of  $\sim 74$ , 58, 48, and 33% are presented in Fig. 4. It clearly demonstrates that the dependence of the ferroelectric properties on the volume fractions of the PZT phase. As the fractions of the PZT phase decrease, the saturation polarization  $P_s$  and remnant polarization  $P_r$  decrease accordingly for the nanocomposite films. That is attributed to the effect of the paraelectric NZFO layers increasing gradually. Except that the  $P$ – $E$  hysteresis loop of the composite thin film of 33% PZT is somewhat like banana shape [20], the other composite thin films show the ferroelectric behavior at an applied maximum electric field of 400 kV/cm. Compared with the  $P$ – $E$  curve of the pure PZT film by the same processing, (shown in the inset of Fig. 4,  $P_r = 18.15 \mu\text{C}/\text{cm}^2$ ,  $P_s = 41.91 \mu\text{C}/\text{cm}^2$ , and  $E_c = 44.26 \text{ kV}/\text{cm}$ ), those of the multilayer thin films seem to show reduced  $P_r$ ,  $P_s$  and high coercive field  $E_c$ . It should be understood that magnetic ferrite NZFO phase with low resistance tends to cause an increase of the leakage current in composite film. Because of this, the actually applied electric field during the measurement should be larger than effective electric fields that switch the domains. As a result, the obtained  $E_c$  value seems higher. For different composite films, the  $E_c$  values might be affected somewhat by the volume fraction of piezoelectric phase. But, this will not influence the calculation of  $P_r$  and even the following magnetic–electric properties. The ferroelectric and magnetic parameters of these films are listed in Table 1. The composite film with the PZT volume fractions of  $\sim 48\%$  exhibits good



**Fig. 2** XRD patterns of the PZT–NZFO multilayered thin film and single-phase PZT and NZFO films on the Pt/Ti/SiO<sub>2</sub>/Si substrate



**Fig. 3** SEM images of the surfaces of **a** the NZFO film and **b** the PZT film and the cross-sections of **c** the NZFO film and **d** the PZT film and **e**, **f** the PZT–NZFO multilayered thin films

ferroelectric and magnetic properties. Compared with other composite films, it possesses higher  $P_s$ ,  $P_r$ ,  $M_s$ , and  $M_r$  and lower  $E_c$  and  $H_c$ .

The composite thin films with four different volume fractions of PZT phase of ~74, 58, 48, and 33% exhibit a well-defined magnetic hysteresis loops as shown in Fig. 5. Here, it should be noted that the magnetizations shown in the figure are calculated by using the whole volumes of the composite films. All composite thin films exhibit good magnetic properties, that is, the high saturation magnetization  $M_s$  and low coercive magnetic field  $H_c$ . It is noteworthy that the  $H_c$  of all the composite thin films are lower than that of the single-phase NZFO film. According to piezomagnetic effect [12, 21], the stress  $\sigma$  facilitates the magnetization when the product of stress  $\sigma$  and magnetostriction  $\lambda_s$  is positive, ( $\sigma \cdot \lambda_s > 0$ ). The large compressive strain in the NZFO phase caused by the lattice mismatch and different coefficient of thermal expansion between the PZT and NZFO phases is in favor of the magnetization,

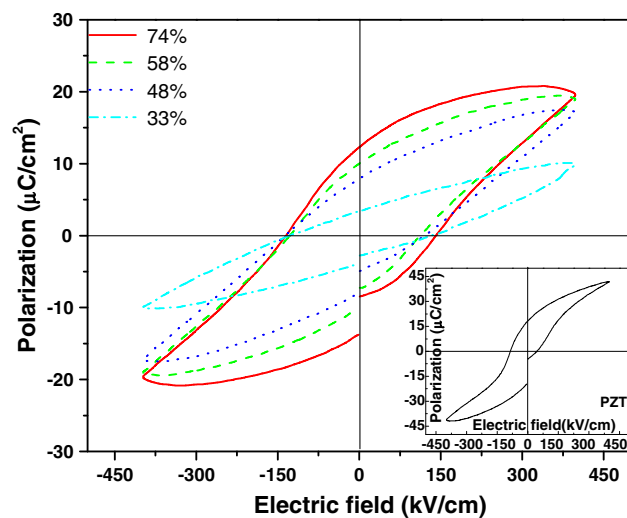


**Fig. 4** Room-temperature  $P$ – $E$  hysteresis loops of the PZT–NZFO nanocomposite films with different volume fractions of PZT phase. The inset is  $P$ – $E$  hysteresis loop of the PZT film

**Table 1** The magnetic and electric parameters of the PZT–NZFO composite thin films with the different volume fractions of PZT phase

Composite films and single-phase film A: PZT, B: NZFO	Volume fractions of PZT phase (%)	$P_s$ ( $\mu\text{C}/\text{cm}^2$ )	$P_r$ ( $\mu\text{C}/\text{cm}^2$ )	$E_c$ (kV/cm)	$M_s$ ( $\text{emu}/\text{cm}^3$ )	$M_r$ ( $\text{emu}/\text{cm}^3$ )	$H_c$ (Oe)
Pure PZT	100	41.91	18.15	44.26	—	—	—
$\text{A}_4\text{B}_1\text{A}_4\text{B}_1\text{A}_1$	74	21	12.15	141	174.09	—	—
$\text{A}_4\text{B}_2\text{A}_4\text{B}_2\text{A}_1$	58	19.63	9.98	111.8	178.99	3.00	8.24
$\text{A}_4\text{B}_3\text{A}_4\text{B}_3\text{A}_1$	48	17.36	7.93	118	185.27	11.39	17.70
$\text{A}_2\text{B}_3\text{A}_2\text{B}_3\text{A}_1$	33	10.43	3.33	130.8	268.74	12.16	20.36
Pure NZFO	0	—	—	—	290.26	47.28	63.74

because the  $\lambda_s$  of polycrystalline Ni–Zn ferrite is negative. This easy-magnetization characteristic is very helpful for the magnetic domain rotation consequently which leads to the enhancement of magnetoelectric coupling in the composite films even at a very low magnetic field. As the volume fractions of the NZFO phase increase, the  $M_s$  and  $H_c$  increase correspondingly. This indicates that the magnetization of the multilayered films is affected by the NZFO ferrite phase.

The coexistence of the ferromagnetic NZFO and ferroelectric PZT phase in the composite thin films gives rise to ME effect. The ME coefficient ( $\alpha_E = dE/dH$ ) was measured according to the variation of the  $\alpha_E$  as a function of the  $H_{dc}$ . Figure 6 shows the ME properties of the composite thin films with different volume fractions of the PZT phase. The composite thin film with 48% PZT exhibits the maximum ME voltage coefficient of 278 mV/cmOe which is much larger than those of the bulk composites such as ferrite/piezoelectric ceramics (e.g., Ni–ferrite/PZT (115 mV/cmOe),  $\text{Ni}_{0.8}\text{Zn}_{0.2}\text{Fe}_2\text{O}_4/\text{Sr}_{0.5}\text{Ba}_{0.5}\text{Nb}_2\text{O}_6$  (26.6 mV/cmOe),  $\text{CoFe}_2\text{O}_4/\text{PZT}$  (30.2 mV/cmOe) composites) [14, 22, 23]. Compared

with the  $H_c$  of general bulk ferrites (including  $\text{CoFe}_2\text{O}_4$ , Ni–ferrite), that of NZFO ferrite phase within our sample exhibits lower value [24–26]. Such soft magnetic characteristics imply that the domain wall motion and the domain rotation are easy, which results in a large magnetostriction  $\lambda$  at low magnetic field and thus leads to a high  $\alpha_E$  value [8]. Besides, we all know that the piezoelectric performance of PZT phase is much better than many piezoelectric ceramics like  $\text{Sr}_{0.5}\text{Ba}_{0.5}\text{Nb}_2\text{O}_6$ , which is also helpful for achieving high  $\alpha_E$  value within the composite ME film. With  $H_{dc}$  increasing to 250 Oe, the  $\alpha_E$  reaches the maximum then drops rapidly for the composite thin films with 48 and 58% volume fractions of PZT phase. For the other two composite thin films, the variation of  $\alpha_E$  with  $H_{dc}$  decrease slowly. We note that the dependence of  $\alpha_E$  on  $H_{dc}$  tracks the  $H_{dc}$  dependence of the piezomagnetic coupling coefficient  $q = \delta\lambda/\delta H_{dc}$  [8]. Once the magnetostriction  $\lambda$  of the ferrite attains the saturation value, the  $q$  will decrease and the piezomagnetic coupling will become weak gradually, which leads to the decrease of the ME effect [8, 27]. In addition, the composite thin films with volume fractions of PZT phase of 33% have the lowest  $\alpha_E$  due to its high ratio of low resistive

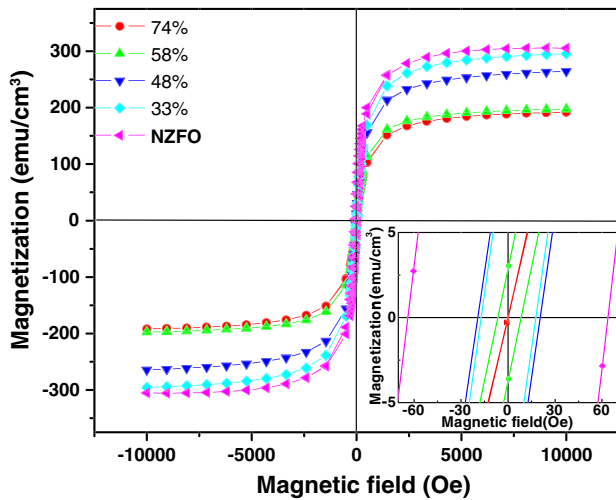


**Fig. 5** Room-temperature magnetic hysteresis loops of the PZT–NZFO nanocomposite films. The inset shows the enlarged parts for the loops near zero field

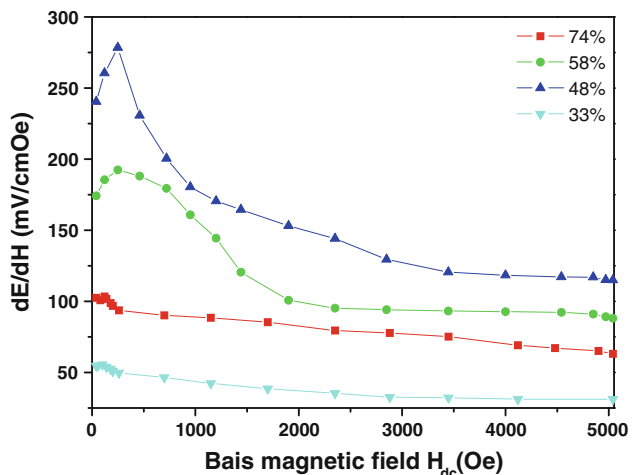


**Fig. 6** ME coupling characteristics of the PZT–NZFO films with different volume fractions of the PZT phase

magnetic layers. We observe that the optimum  $H_{dc}$  where  $\alpha_E$  reaches the maximum value appears within the range of 80–250 Oe. As discussed above, such low values for the optimum  $H_{dc}$  can be attributed to the easy-magnetization characteristics of the NZFO phase.

## Conclusions

The magnetoelectric PZT–NZFO composite thin films with different volume fractions of PZT phase were manufactured using sol–gel process and spin-coating technique. SEM images indicate that the composite thin films have a multilayered nanostructure. For the composite films, the magnetization properties degrade and the ferroelectric properties increase as the fraction of PZT phase increases. The composite thin film with volume fractions of PZT phase of 48% exhibits good coexistence of ferroelectric and ferromagnetic properties with the  $P_s \sim 17.36 \mu\text{C}/\text{cm}^2$  and  $M_s \sim 185.27 \text{ emu}/\text{cm}^3$ , as well as the maximum  $\alpha_E$  of 278 mV/cmOe.

**Acknowledgements** This study was supported by the Specialized Research Fund for the Doctoral Program of Higher Education (Grant No. 200803591037) and partially by the National Natural Science Foundation of China (50972035) and a Program for New Century Excellent Talents in University, State Education Ministry (NCET-08-0766).

## References

- Bichurin MI, Petrov VM, Kiliba YV (2002) Phys Rev B 66:134404
- Eerenstein W, Mathur ND, Scott JF (2006) Nature 442:759
- Wang YJ, Zhao XY, Jiao J, Zhang QH, Di WN, Luo HS, Leung CM, Or SW (2010) J Alloys Compd 496:L4
- Zeng M, Or SW, Chan HLW (2010) J Alloys Compd 490:L5
- Zhang JX, Dai JY, Chow CK, Sun CL, Lo VC, Chan HLW (2008) Appl Phys Lett 92:022901
- Dix N, Skumryev V, Laukhin V, Fàbrega L, Sánchez F, Fontcuberta J (2007) J Mater Sci Eng B 144:127
- Yi SW, Kim SS, Kim JW, Jo HK, Do D, Kim WJ (2009) Thin Solid Films 517:6737
- Wan JG, Wang XW, Wu YJ, Zeng M, Wang Y, Jiang H, Zhou WQ, Wang GH, Liu JM (2005) Appl Phys Lett 86:122501
- Srinivasan G, DeVreugd CP, Hayes R, Bichurin MI, Petrov VM (2004) Magnetoelectr Interact Phenom Cryst 164:35
- Ma YG, Cheng WN, Ning M, Ong CK (2007) Appl Phys Lett 90:152911
- Levin I, Li JH, Slutsker JL, Roytburd AL (2006) Adv Mater 18:2044
- He HC, Wang J, Zhou JP, Nan CW (2007) Adv Funct Mater 17:1333
- Delgado E, Ostos C, Martínez-Sarrión ML, Mestres L, Lederman D, Prieto P (2009) Mater Chem Phys 113:702
- Li YJ, Chen XM, Lin YQ, Tang YH (2006) J Eur Ceram Soc 26:2839
- Guo YY, Zhou JP, Liu P (2010) Curr Appl Phys 10:1092
- Jo HK, Kim SS, Do D (2009) J Sol-Gel Sci Technol 49:336
- He HC, Zhou JP, Wang J, Nan CW (2006) Appl Phys Lett 89:052904
- Deng CY, Zhang Y, Ma J, Lin YH, Nan CW (2007) J Appl Phys 102:074114
- Fina I, Dix N, Laukhin V, Fàbrega L, Sánchez F, Fontcuberta J (2009) J Magn Magn Mater 321:1795
- Scott JF (2008) J Phys Condens Matter 20:021001
- O’Handley RC (2000) Modern magnetic materials: principles and applications, chap 7. Wiley, New York
- Zhai JY, Cai N, Liu L, Lin YH, Nan CW (2003) Mater Sci Eng B 99:329
- Ryu J, Priya S, Uchino K, Kim H (2002) J Electroceram 8:107
- Zi ZF, Lei HC, Zhu XD, Wang B, Zhang SB, Zhu XB, Song WH, Sun YP (2010) Mater Sci Eng B 167:70
- Sathaye SD, Patil KR, Kulkarni SD, Bakre PP, Pradhan SD, Sarwade BD, Shintre SN (2003) J Mater Sci 38:29. doi:[10.1023/A:1021101529855](https://doi.org/10.1023/A:1021101529855)
- Huang XH, Chen ZH (2004) J Magn Magn Mater 280:37
- Zeng M, Wan JG, Wang Y, Yu H, Liu JM, Jiang XP, Nan CW (2004) J Appl Phys 95:8069